Textures and Microstructures, Vol. 34, pp. 181–195
Reprints available directly from the publisher
Photocopying permitted by license only

THE EVOLUTION OF TEXTURE DURING ANNEALING OF NANOCRYSTALLINE ELECTROLESS NICKEL ALLOY DEPOSITS

DONG NYUNG LEE[a,*] and KANG-HEON HUR[b]

[a]*School of Materials Science and Engineering, Seoul National University, Seoul 151-742, Korea;* [b]*Materials Research Laboratory, R & D Center, Samsung ElectroMechanics, Suwon 442-743, Korea*

(Received 8 October 1999)

The electroless Ni–Co–P alloy films containing up to 13.4% Co and 7.6% P were deposited on a 5086 aluminum alloy sheet using baths consisting of $NiSO_4$, $CoSO_4$, $(NH_4)_2SO_4$, NaH_2PO_2, sodium citrate and thiourea. The deposits were solid solutions having a grain size of 6–7 nm and strong ⟨111⟩ texture. When the deposits were annealed for 2 h, Ni_5P_2 was precipitated at 325°C and transformed into the stable Ni_3P phase at higher temperatures. During annealing the texture of deposit changed from ⟨111⟩ to ⟨100⟩. The texture change was attributed to preferential growth of ⟨100⟩ grains at the expense of ⟨111⟩ grains to decrease the thermal strain energy of the deposits. On the other hand, the electroless Ni–Cu–P alloy films containing Cu and P deposited on 5086 aluminum alloy sheet had the microstructures and textures which are similar to these of the Ni–Co–P alloy films. However, their initial ⟨111⟩ texture remained relatively stable even after annealing. The differences in annealing textures of Ni–Co–P and Ni–Cu–P alloy films have been discussed.

Keywords: Electroless nickel alloy; Deposition texture; Annealing texture; Nanocrystalline

INTRODUCTION

The Ni–Co–P alloy deposits can be obtained from alkaline solutions over entire Co compositions (Pearlstein, 1974). The deposits with higher Co concentrations are applied to magnetic recording media and vertical

* Corresponding author.

magnetic recording media by adding Mn and Re (Osaka *et al.*, 1983a,b; Koiwa and Osaka, 1987). The increase in the Co concentration causes the decrease in the P content and the increase in grain size (Chow *et al.*, 1972). Little study has been made of texture changes during annealing of the Ni–Co–P alloy deposits (Lee and Hur, 1999). Microstructures and crystallization of the electroless Ni–P deposits and magnetic properties and microstructures of electroless Ni–Cu–P deposits were studied by the present authors (Park and Lee, 1988; Hur *et al.*, 1990; 1991).

In this paper, the evolution of texture and phase transformation behavior during annealing of the Ni–Co–P and Ni–Cu–P deposits have been discussed.

EXPERIMENTAL PROCEDURE

The electroless Ni–Co–P alloy films were deposited on a 5086 aluminum alloy sheet which had been preplated. The preplating process included cleaning, and nitric acid and double zincating treatments. The zincating treatments are performed to remove oxide film formed after alkali cleaning and acid etching, to prevent reoxidation and to form catalytic surface, which is necessary for electroless nickel plating. The bath used to obtain the electroless deposits consisted of 0.07–0.1 mol/l $Ni^{2+}(NiSO_4)$, 0–0.03 mol/l Co^{2+} ($CoSO_4$), 0.5 mol/l $(NH_4)_2SO_4$, 0.2 mol/l NaH_2PO_2, 0.2 mol/l sodium citrate and 1 ppm thiourea. Ammonia solution was used to adjust the pH of the bath to 9.0. The temperature of the bath was maintained at 90°C with a thermoregulator and agitated by magnetic stirring.

The thickness of deposits ranged from 30 to 40 μm. The P and Co contents in the deposits were analyzed by the inductively coupled plasma (ICP) emission spectrometry. Adherence between the electroless deposit and the aluminum substrate depends on the zinc layer thickness. If the thickness is too thick, peeling occurs between the deposit and the substrate. The appropriate thickness is known to be about 100 nm. Changes in structures of as-deposited and heat-treated films were measured by the usual continuous scanning X-ray diffraction method. The heat treatment of the deposits used in X-ray diffraction was carried out isothermally in a salt bath for 2 h at temperatures from 250°C to 450°C with 50°C intervals. The diffusion depth due to 100 nm thick zinc

layer was estimated to be less than 1 μm when the deposits are heated at 4500°C for 2 h, and the thickness of deposits ranged from 30 to 40 μm. Therefore, the X-ray diffraction results were not influenced by the zinc layer. The structure analysis and heat treatments of the films were conducted without being separated from the substrate.

RESULTS AND DISCUSSION

Deposition Rate and Composition

Figure 1 shows the deposition rate of the electroless In–Co–P deposit as a function of $[CO^{2+}]/[Ni^{2+}]$ in deposition solution. The deposition rate remained constant until a cobalt ion to nickel ion ratio of 0.1, beyond which the deposition rate decreased slowly with increasing ratio. Figure 2 shows the cobalt and phosphorous contents of the deposits as a function of $[Co^{2+}]/[Ni^{2+}]$ in the deposition solution. The cobalt content in the deposit increased with increasing ratio of $[Co^{2+}]/[Ni^{2+}]$. However, the increasing rate of cobalt content in the deposit was not so large as the increasing rate of cobalt ion in the solution.

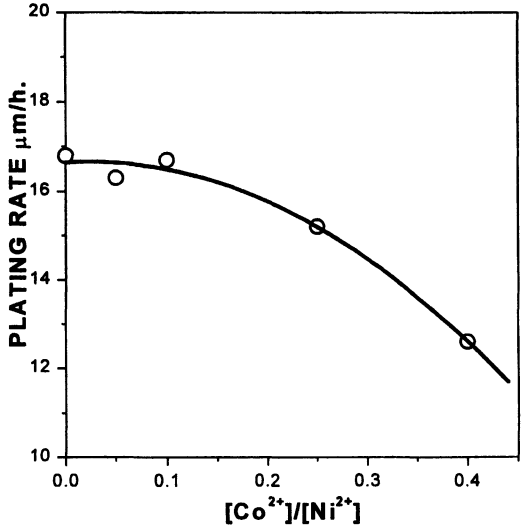

FIGURE 1 Plating rate of electroless Ni–Co–P deposit as a function of $[Co^{2+}]/[Ni^{2+}]$ in solution.

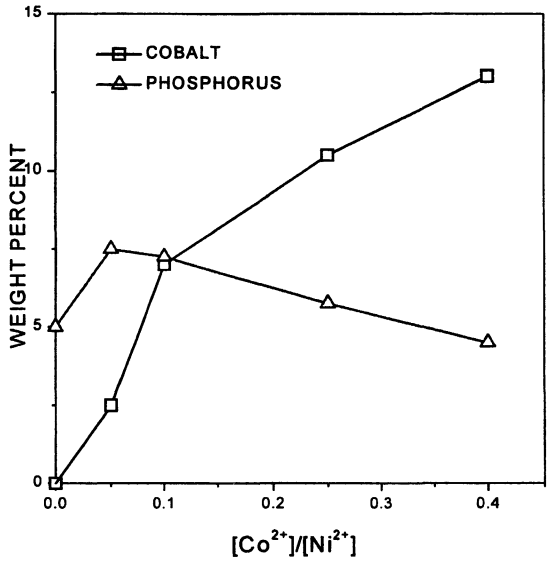

FIGURE 2 Cobalt and phosphorous content in electroless Ni–Co–P deposit as a function of $[CO^{2+}]/[Ni^{2+}]$ in solution.

The phosphorous content in the deposit increased initially and decreased slowly with increasing $[Co^{2+}]/[Ni^{2+}]$ ratio.

Microstructures and Textures of Deposits

Transmission electron micrographs (dark field image) and diffraction patterns of various electroless Ni–Co–P deposits are shown in Fig. 3. The micrographs indicate that fine grains are imbedded in amorphous matrix. The amorphous phase is supposed to have a higher phosphorous content than crystalline grains from the well known fact that the electroless Ni–P deposits tend to become amorphous with increasing phosphorous content. X-ray diffraction patterns of electroless Ni–Co–P alloy deposits in Fig. 4(a) shows strong (111) and very weak (200) reflection peaks, which indicate that the deposits have the ⟨111⟩ texture. Their grain size is estimated to be 6–7 nm by the Scherrer equation. This size is approximately the same as that of white spots as in Fig. 3. It can be seen that the (200) peak intensity relative to the (111) peak increases with increasing cobalt content in the deposits. The Ni–5.1P deposit also shows the (200) peak.

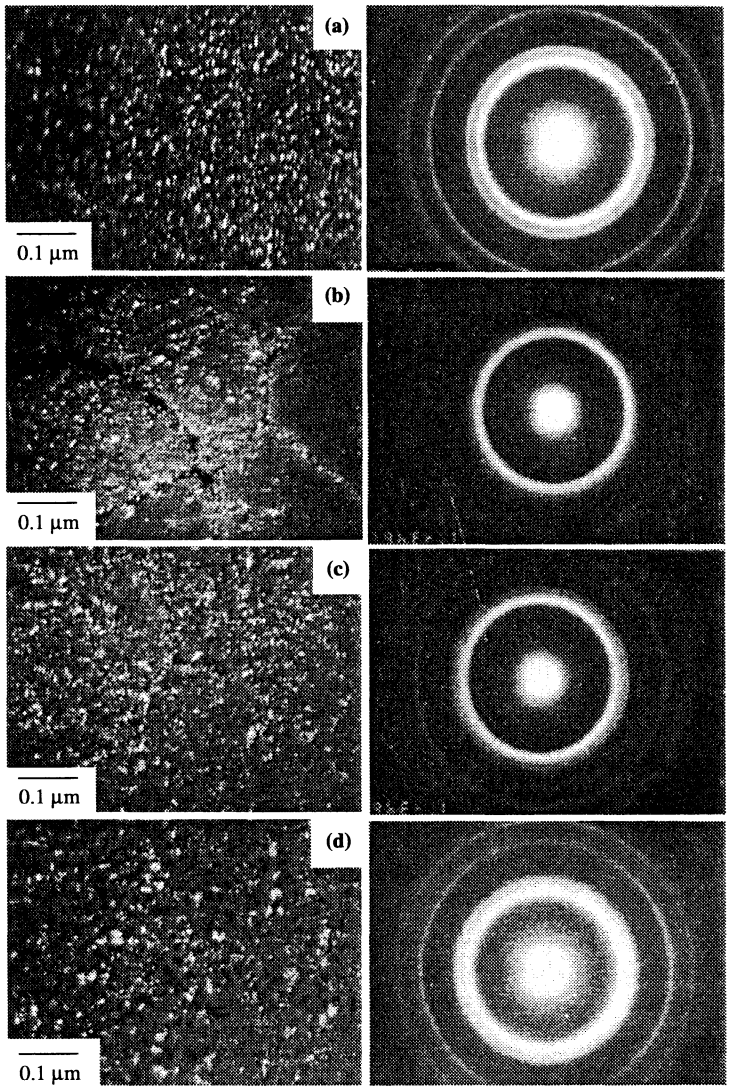

FIGURE 3 Dark field micrographs and SAD patterns of electroless Ni–Co–P deposits. (a) Ni–2.4Co–7.6P, (b) Ni–7.0Co–7.2P, (c) Ni–10.5Co–5.8P, (d) Ni–13.4Co–4.5P.

Annealing Effects

Figure 4 shows X-ray diffraction patterns of electroless Ni–Co–P deposits annealed at various temperatures for 2 h. The (200) peak intensity increases more rapidly than the (111) intensity with increasing annealing temperature and cobalt content in the deposits. At an annealing temperature of 325°C, Ni_5P_2 forms especially in the higher phosphorous deposits, but it disappears and stable Ni_3P appeared at higher temperatures. A similar phenomenon was observed in electroless Ni–Cu–P alloys (Hur *et al.*, 1991). The appearance of Ni_5P_2 from the annealed Ni–Cu–P deposit was attributed to a higher phosphorous segregation in grain boundary region. When annealed, the higher phosphorous region was supposed to be further increased by extraction of P dissolved in nickel grains which in turn gave rise to precipitation of the Ni_5P_2 phase. The same explanation may be applicable to the Ni–Co–P deposits.

The evolution of ⟨100⟩ in a fcc metal film with ⟨111⟩ orientation on a substrate during annealing can originate from a few sources. A lattice matching at the film–substrate interface may lead to the ⟨100⟩ orientation. But there is little possibility of lattice matching between the substrate and the nickel alloy deposit.

When ⟨111⟩ fcc copper electrodeposits (Lee *et al.*, 1995; Lee, 1996a,b) and silver electrodeposits (Nam and Lee, 1999) were recrystallized, the ⟨100⟩ orientation developed (Lee *et al.*, 1995; Lee, 1996a,b). However, this is possible when the dislocation density in the deposit is high enough to cause recrystallization. Since the present deposits have a grain size of several nanometer, they are likely to have little dislocation. Therefore, the explanation cannot be applied to this system.

The texture evolution during annealing may be due to grain growth. A duplex texture of ⟨111⟩ and ⟨100⟩ in fcc metals tends to develop ⟨111⟩ during grain growth. The grain boundaries in a material with a duplex fiber texture of ⟨111⟩ and ⟨100⟩ may be described approximately as tilt boundaries of ⟨111⟩ and ⟨100⟩ grains and boundaries between ⟨111⟩ and ⟨100⟩ grains as shown in Fig. 5. The ⟨111⟩–⟨100⟩ boundaries will not determine which grains grow favorably. If the tilt boundary energies of the two differently textured grains are different, the grains with lower boundary energy will grow at the expense of the grains with the higher boundary energies when the mobilities of the grain boundaries

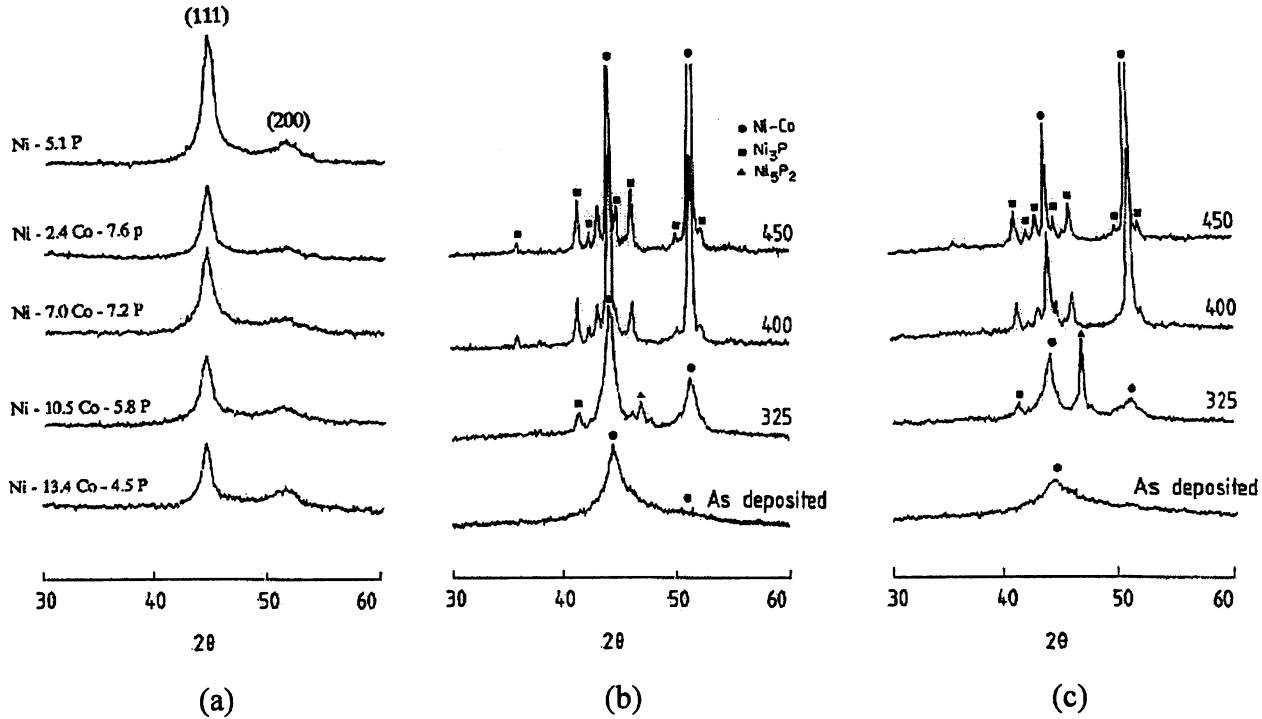
(111)
(200)
Ni - 5.1 P
Ni - 2.4 Co - 7.6 p
Ni - 7.0 Co - 7.2 P
Ni - 10.5 Co - 5.8 P
Ni - 13.4 Co - 4.5 P
30
40
50
60
2θ
(a)
Ni-Co
Ni3P
Ni5P2
450
400
325
As deposited
30
40
50
60
2θ
(b)
450
400
325
As deposited
30
40
50
60
2θ
(c)

FIGURE 4(a)–(c)

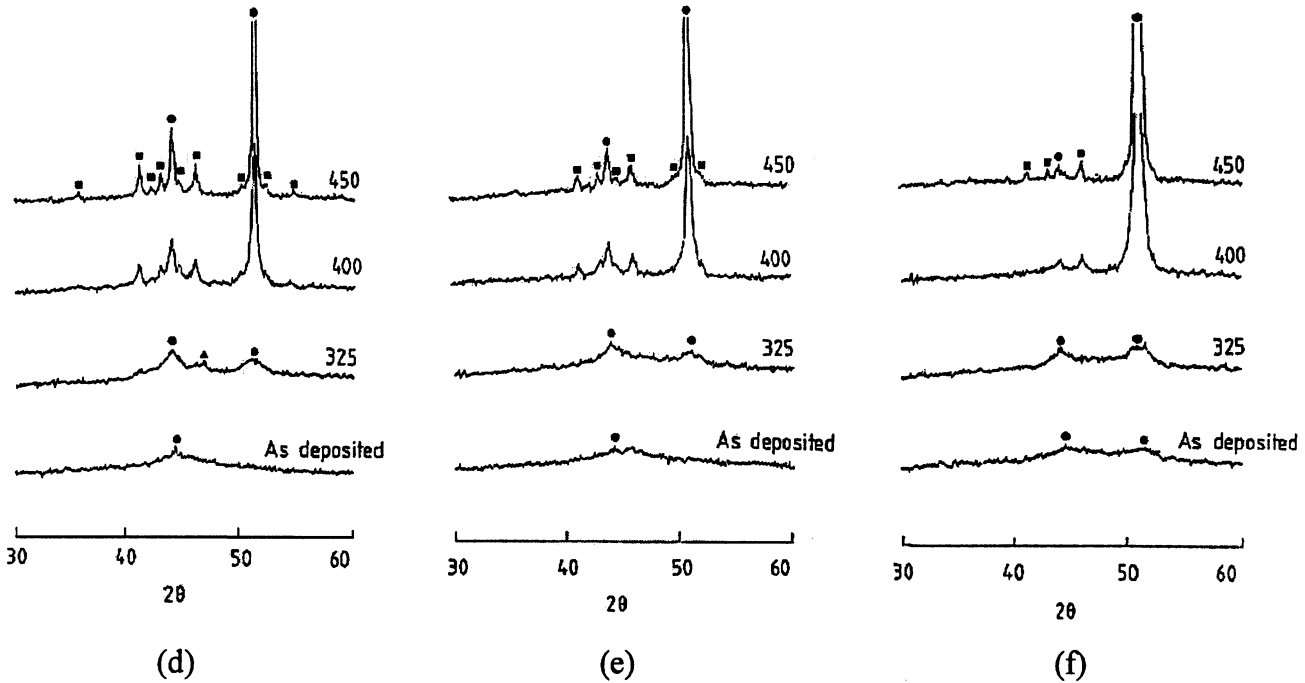

FIGURE 4(d)–(f)

FIGURE 4 X-ray diffraction patterns of electroless Ni–Co–P deposits. (a) as-deposited, (b) Ni–5.1P, (c) Ni–2.4Co–7.6P, (d) Ni–7.0Co–7.2P, (e) Ni–10.5Co–5.8P and (f) Ni–13.4Co–4.5P are annealed at various temperatures for 2 h. Peak intensities in (b) to (f) are attenuated.

are the same. For copper and gold, the calculated average boundary energy of ⟨111⟩ grains is slightly higher than ⟨100⟩ grains as shown in Fig. 6 (Wolf, 1990). For aluminum, the mobility of tilt grain boundaries of ⟨111⟩ grains is higher than that of ⟨100⟩ grains at high temperatures as shown in Fig. 7 (Aleshin *et al.*, 1978). In this case, neighboring ⟨111⟩ grains will grow faster than neighboring ⟨100⟩ grains, resulting in the ⟨111⟩ grain size being larger than the ⟨100⟩ grain size. The ⟨111⟩ grains will grow at the expense of the ⟨100⟩ grains because of the size advantage, and develop the ⟨111⟩ texture during grain growth. Indeed, nanocrystalline Fe–Ni alloy electrodeposits developed the ⟨111⟩ texture when annealed (Czerwinski *et al.*, 1997). The recrystallization textures of silver (Shin *et al.*, 2000) and copper (Backofen, 1952) wires are ⟨100⟩, whereas their growth textures are ⟨111⟩ (Shin *et al.*, 2000; Grant *et al.*, 1984). Therefore, the ⟨100⟩ annealing texture in this study cannot be caused by grain growth.

The texture change from ⟨111⟩ to ⟨100⟩ may be due to the fact that the ⟨111⟩ grains have the highest strain energy while the ⟨100⟩ grains the

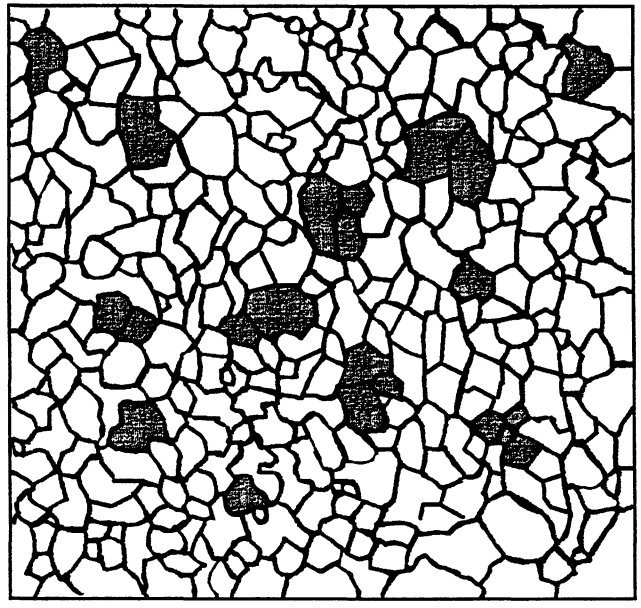

FIGURE 5 Schematic microstructure of section normal to growth direction of deposit which consists of ⟨111⟩ grains and ⟨100⟩ grains (dark).

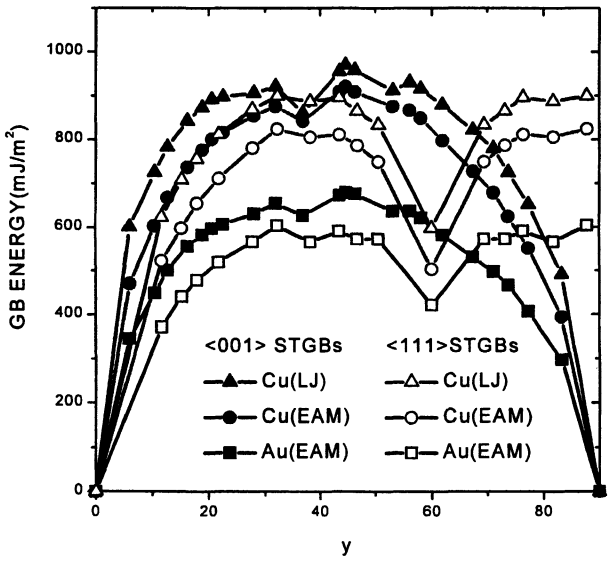

FIGURE 6 Calculated energy (in mJ/m^2) for symmetrical tilt grain boundaries of fcc metals with interface planes perpendicular to ⟨111⟩ and ⟨100⟩ as function of tilt angle (Wolf, 1990). (LJ and (EAM) indicate energies have been calculated using LJ and EAM potentials.)

lowest strain energy (Carel *et al.*, 1996). The deposit and substrate, which have different thermal expansion coefficients, undergo different volume changes due to a temperature change. In addition, the formation of nickel phosphide could lead to volume changes. These changes can produce strains and in turn stresses in the deposits during annealing. The experimental results (Fig. 4) indicate that the texture change is more influenced by cobalt concentration than by phosphorous. This implies that the volume changes due to phosphide formation are not a dominant factor leading to the ⟨100⟩ texture. Therefore this factor is not considered here.

The strains and stresses due to the different thermal expansion coefficients are calculated. The thermal strain ε_{th} due to the different thermal expansions is calculated by

$$\varepsilon_{th} = \int_{T_0}^{T} (\alpha_s - \alpha_f)\, dT \tag{1}$$

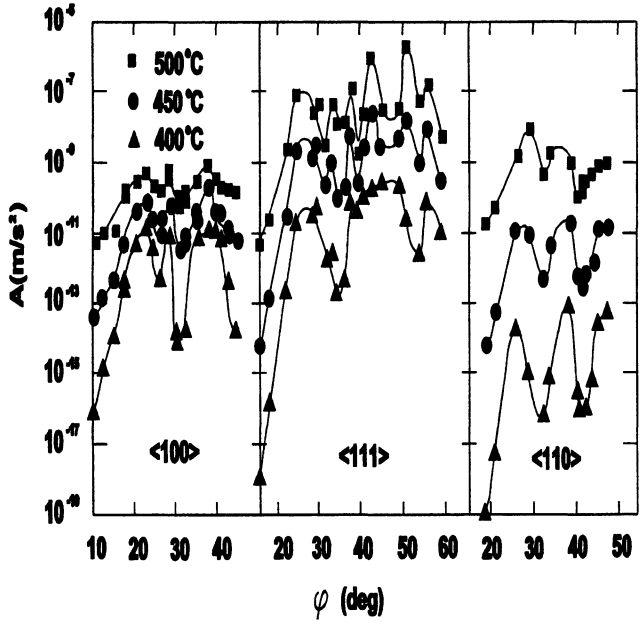

FIGURE 7 Misorientation dependence of the tilt grain boundary mobility in aluminum of misorientation axes ⟨100⟩, ⟨110⟩ and ⟨111⟩ (Aleshin *et al.*, 1978).

where T and α are temperature and thermal expansion coefficient, respectively. Subscripts 0, s and f indicate initial state, substrate and film, respectively. Setting $T = 250$–$450°C$, $T_0 = 90°C$, $\alpha_s = \alpha_{Al} = 25.8 \times 10^{-6} K^{-1}$ (Metals Handbook, 1979), $\alpha_f = \alpha_{Ni} = 13.3 \times 10^{-6} K^{-1}$ (Metals Handbook, 1979), we obtain

$$\varepsilon_{th} = (2 \text{ to } 4.5) \times 10^{-3} \tag{2}$$

To be more rigorous, the thermal expansion coefficients of fcc Ni–Co solid solutions should be used. The thermal expansion coefficient of cobalt (hcp) is $13.8 \times 10^{-6} K^{-1}$ (Metals Handbook, 1979) which is very close to that of nickel. Therefore, the thermal expansion coefficient of nickel can be a good approximation of the alloys in the absence of experimental values.

A polycrystalline deposit which has a strong fiber texture is expected to have a normal anisotropy, even though each grain may not have the

normal anisotropy. Therefore, the stress state of deposit can be approximated by an equibiaxial plane stress state, which may be expressed as $\sigma_{11}=\sigma_{22}=\sigma$ and $\sigma_{12}=0$. It follows from the generalized Hooke's law for anisotropic materials that

$$\varepsilon_{11} = S'_{1111}\sigma'_{22} = (S'_{1111} + S'_{1122})\sigma \tag{3}$$

where the prime means the quantity along an arbitrary axis in plane and S_{ijkl} is the compliances. Using the transformations law, the following equations are obtained for cubic crystals

$$\sigma = \frac{\varepsilon'_{11}}{S_{11} + S_{12}} \quad \text{for } \{100\} \text{ planes} \tag{4}$$

$$\sigma = \frac{\varepsilon'_{11}}{S_{11} + S_{12} + (1/6)(S_{44} - 2S_{11} + 2S_{12})} \quad \text{for } \{111\} \text{ planes} \tag{5}$$

$$\sigma = \frac{E}{1 - \nu_{11}}\varepsilon'_{11} \quad \text{for isotropic materials} \tag{6}$$

where E and ν are Young's modulus and Poisson's ratio, respectively. The above stresses are independent of x'_1 direction, which in turn means that ε'_{11} is also independent of x'_1 direction. That is, the above equations hold for the equibiaxial strain state. It follows that

$$\sigma_{\text{th}}(100) = \frac{\varepsilon_{\text{th}}}{S_{11} + S_{12}} \tag{7}$$

$$\sigma_{\text{th}}(111) = \frac{\varepsilon_{\text{th}}}{S_{11} + S_{12} + (1/6)(S_{44} - 2S_{11} + 2S_{12})} \tag{8}$$

$$\sigma_{\text{th}}(\text{iso}) = \frac{E}{1 - \nu}\varepsilon_{\text{th}} \tag{9}$$

where $\sigma_{\text{th}}(100)$, $\sigma_{\text{th}}(111)$ and $\sigma_{\text{th}}(\text{iso})$ indicate thermal stresses of the film having (100), (111) and random orientations, respectively.

Setting $S_{11} = 0.00734$, $S_{44} = 0.00802$, $S_{12} = -0.00274\,\text{GPa}^{-1}$ (Reid, 1973), $E = 201$, and $v = 0.31$, $\sigma_{th}(100) = 217 \times (2\text{–}4.5)\,\text{MPa}$, $\sigma_{th}(111) = 388 \times (2\text{–}4.5)\,\text{MPa}$ and $\sigma_{th}(\text{iso}) = 291 \times (2\text{–}4.5)\,\text{MPa}$. $\sigma_{th}(100)$ is lower than $\sigma_{th}(111)$. Therefore, the ⟨100⟩ grains have lower strain energy than the ⟨111⟩ grains. These values are based on room temperature data. The stresses at experimental temperatures of 250–450°C would be lower, but still substantial. In conclusion, the evolution of the ⟨100⟩ orientation during annealing is suggested to be due to favorable growth of ⟨100⟩ grains at the expense of ⟨111⟩ grains under thermal stresses.

Electroless Ni–Cu–P deposits showed similar grain size and textures at the initial state, but the ⟨111⟩ texture remained relatively stable even after annealing within the experimental range as shown in Fig. 8 (Hur *et al.*, 1991). The thermal expansion coefficient of copper (19.6×10^{-6} at 700 K (Metals Handbook, 1979)) is higher than that of cobalt.

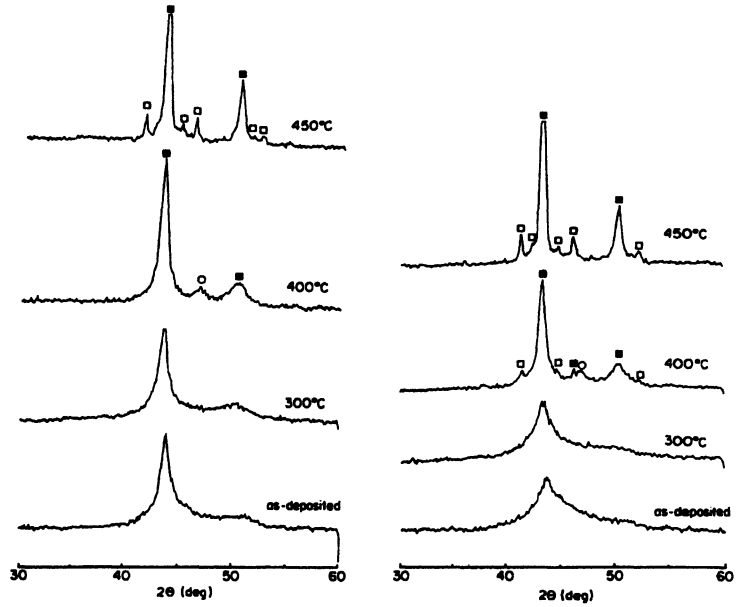

FIGURE 8 X-ray diffraction patterns of electroless (a) Ni–44.5Cu–7.5P and (b) Ni–50.3Cu–5.7P deposits. Annealing was performed at 300°C, 400°C and 450°C for 2 h.

Therefore, the less thermal stress would be developed, resulting in the slower evolution of the ⟨100⟩ orientation.

CONCLUSIONS

(1) The plating rate of electroless Ni–Co–P alloys decreased with increasing ratio of cobalt ion concentration to nickel ion concentration in bath.
(2) The phosphorous content in the deposit slightly decreased with increasing cobalt content.
(3) When the deposit was annealed for 2 h, Ni_5P_2 was precipitated at 325°C and replaced by stable Ni_3P at higher temperatures.
(4) The as-deposited Ni–Co–P films had strong ⟨111⟩ texture, which changed to the ⟨100⟩ texture on annealing. The rate of texture change increased with increasing cobalt concentration. The texture change was due to preferential growth of ⟨100⟩ grains at the expense of ⟨111⟩ grains to reduce the thermal strain energy of the deposits.
(5) The Ni–Cu–P films had the texture and microstructure similar to the Ni–Co–P films. However, the texture remained relatively stable possibly due to the less thermal stresses.

Acknowledgement

This study has been supported by National Research Laboratory for Texture Control, Seoul National University.

References

Aleshin, A.X., Aristov, V.Y., Bokstein, B.S. and Shvindlerman, L.S. (1978). Kinetic properties of 111 direction tilt boundaries in aluminium. *Phys. Stat. Sol. A*, **45**, 359.

Backofen, W.A. (1952). Recrystallization textures in copper wire. *Trans. Amer. Inst. Min. Met. Eng.*, **194**, 735–54.

Carel, R., Thompson, C.V. and Frost, H.J. (1996). Computer simulation of strain energy effects vs. surface and interface energy effects on grain growth in thin films. *Acta Mater.*, **44**, 2479–94.

Chow, S.L., Hedgecock, N.E., Schiesinger, M. and Rezek, J. (1972). Electron microscope study of the nucleation and growth of electroless cobalt and nickel. *J. Electrochem. Soc.*, **119**, 1614.

Czerwinski, F., Li, H., Megret, M. and Szpunar, J.A. (1997). The evolution of texture and grain size during annealing of nanocrystalline Ni–45%Fe electrodeposits. *Scripta Metall. Mater.*, **37**, 1967–72.

Grant, E., Jensen, D.J., Ralph, B. and Hansen, N. (1984). Texture development during grain growth in pure copper. In *Proc. ICOTOM7*, edited by C.M. Brakman, P. Jongenburger and E.J. Mittemeijer, pp. 239–44. Noordwijkerhout: Netherlands Society for Materials Science.

Hur, K.-H., Jeong, J.H. and Lee, D.N. (1990). Microstructure and crystallization of electroless Ni–P deposits. *J. Mater. Sci.*, **25**, 2573–84.

Hur, K.-H., Jeong, J.H. and Lee, D.N. (1991). Effect of annealing on magnetic properties and microstructure of electroless nickel–copper–phosphorous alloy deposits. *J. Mater. Sci.*, **26**, 2037–44.

Koiwa, I. and Osaka, T. (1987). A study on initial deposition film of electroless plated Co–Ni–R–P alloy for perpendicular magnetic recording media. *J. Met. Fin. Soc. Jpn.*, **38**, 434.

Lee, D.N. and Hur, K.-H. (1999). The evolution of texture during annealing of electroless Ni–Co–P deposits. *Scripta Mater.*, **40**, 1333–9.

Lee, D.N., Kang, S. and Yang, J. (March 1995). Relation between texture and surface morphology of copper electrodeposits. *Plating and Surface Finishing*, **82**, 76–79.

Lee, D.N. (1996a). Maximum energy release theory for recrystallization textures. *Metals and Materials*, **2**, 121–31.

Lee, D.N. (1996b). Texture and related phenomena of copper electrodeposits. *MRS Proc.*, 427, pp. 168–78. *Metals Handbook* 9th edn., Vol. 2, ASM, (1979).

Nam, H.-S. and Lee, D.N. (1999). Recrystallization textures of silver electrodeposits. *J. Electrochem. Soc.*, **146**, 3300–3308.

Osaka, T., Kasai, N., Koiwa, I. and Goto, F. (1983a). A preparation of perpendicular magnetic recording media by an electroless plating method. *J. Electrochem. Soc.*, **130**, 568–71.

Osaka, T., Kasai, H., Koiwa, I. and Goto, F. (1983b). A study on electroless plating of cobalt alloy films for perpendicular recording. *J. Electrochem. Soc.*, **130**, 790–94.

Park, S.H. and Lee, D.N. (1988). A study on the microstructure and phase transformation of electroless nickel deposits. *J. Mater. Sci.*, **23**, 1643–54.

Pearlstein, F. (1974). Electroless plating. In *Modern Electroplating*, 3rd edn., edited by F.A. Lowenheim, pp. 710–47. John Wiley and Sons, Inc.

Reid, C.N. (1973). Deformation geometry for materials scientists, p. 68. Pergamon Press.

Shin, H.-J., Jeong, H.-T. and Lee, D.N. (2000). Deformation and annealing textures of silver wire. *Mater. Sci. Eng. A*, **279**, 245–54.

Wolf, D. (1990). Structure–energy correlation for grain boundaries in fcc metals-III. Symmetrical tilt boundaries. *Acta Metal L. Mater.*, **38**, 781–90.